Available online at www.sciencedirect.com

ScienceDirect

Ceramics International 41 (2015) 6970–6977

CERAMICS INTERNATIONAL

www.elsevier.com/locate/ceramint

Structural dependent room-temperature ferromagnetism in yttrium doped HfO_2 nanoparticles

Z. D. Dohčević-Mitrović[a,*], N. Paunović[a], B. Matović[b], P. Osiceanu[c], R. Scurtu[c,d], S. Aškrabić[a], M. Radović[a]

[a]Institute of Physics, University of Belgrade, Pregrevica 118, 11080 Belgrade, Serbia
[b]Institute of Nuclear Sciences 'Vinča', University of Belgrade, 11000, Serbia
[c]Institute of physical chemistry, Romanian academy, Bucharest 060021, Romania
[d]National Institute for Research and Development in Microtechnologies, Bucharest 060021, Romania

Received 18 September 2014; received in revised form 30 January 2015; accepted 2 February 2015
Available online 7 February 2015

Abstract

Y-doped HfO_2 nanopowders, produced by metathesis synthesis, exhibit ferromagnetism at room temperature. The X-ray diffraction and Raman measurements have shown that HfO_2 nanopowders undergo phase transformation from monoclinic to tetragonal and cubic phase with increasing of Y content. The X-ray photoelectron spectroscopy and Raman analysis gave evidence that Y-doped HfO_2 nanopowders are oxygen deficient. The ferromagnetic properties of Y-doped HfO_2 nanocrystals are dependent on crystal structure changes. The structural transformation from monoclinic to tetragonal phase with Y doping is followed by increased ferromagnetic ordering because of the increased concentration of oxygen vacancies (V_O) in different charge states. Higher Y content favors the formation of cubic phase and the ferromagnetism significantly weakens. In cubic hafnia phase, yttrium can form (V_O–Y_{Hf}) defect complexes in different charge states. The appearance of these complexes can be responsible for the degradation of ferromagnetic ordering.

Keywords: A. Powders: chemical preparation; X-ray method and spectroscopy; Optical and magnetic properties; HfO_2

1. Introduction

Hafnia (HfO_2) is very promising and technologically important material because of potential applications in spintronic devices, high-temperature fuel cells and has attracted much attention as high-*k* dielectric gate material to replace the SiO_2 in metal-oxide-semiconductor devices. HfO_2 has three polymorphs, i.e. monoclinic (M), tetragonal (T) and cubic (C) phase. Under ambient conditions the monoclinic phase of hafnia is stable phase and undergoes transition to tetragonal or cubic phase at high temperature [1]. These last two phases are far more important in technological applications than the low-temperature monoclinic phase. Stabilization of the tetragonal and cubic hafnia phases at room temperature can be achieved by doping with divalent or trivalent cation dopants such as Mg^{2+} or Y^{3+} which brings additional oxygen vacancies in the lattice and stabilize one of two high-temperature phases of hafnia [2,3].

HfO_2 is an insulating oxide and is expected to be nonmagnetic because Hf^{4+} and O^{2-} are not magnetic ions with full or empty f and d shells of Hf^{4+} ion. The discovery of unexpected room-temperature ferromagnetism (RTFM) in undoped monoclinic HfO_2 thin films [4] has opened a path to a new class of ferromagnetic materials which can play important role in new generation of spintronic devices. The magnetic ordering was up to now presumably investigated in monoclinic hafnia thin films and possible mechanism for the observed magnetism is still controversial. Different types of defects like oxygen (V_O) or hafnia vacancies (V_{Hf}) were claimed responsible for the FM in hafnia. The FM ordering in M-phase of HfO_2, proposed by Coey and coworkers [5], can arise from unpaired electrons in bonding molecular orbitals formed by hybridization of hafnium orbitals

*Corresponding author. Tel.: +381 11 3713024; fax: +381 11 3162190.
E-mail address: zordoh@ipb.ac.rs (Z.D. Dohčević-Mitrović).

http://dx.doi.org/10.1016/j.ceramint.2015.02.002
0272-8842/

surrounding a neutral three-coordinated oxygen vacancy. Direct exchange between defect-related molecular orbitals will be ferromagnetic and may be strong if defects are situated in the interface layer [5]. Recent calculations of Glinchuk et al. [6], based on the direct variational method, showed that neutral oxygen vacancies in the vicinity of the film–substrate interface can become magnetic and mediate long range FM order in HfO_2 thin films. Furthermore, theoretical calculations of Muñoz Ramo et al. [7], based on DFT periodic and embedded cluster methods, showed that in monoclinic HfO_2 four-coordinated oxygen vacancies can exist in five different charge states (V^{2+}, V^{+}, V^{0}, V^{-}, and V^{2-}). These defects form localized levels in the hafnia band gap. Some of these states have different electron occupancies and bear different magnetic moments [7]. Contrary to these findings, the first principle calculations [8,9] showed that hafnium vacancies, as cation vacancies, can be responsible for the ferromagnetism in monoclinic HfO_2. The removal of neutral Hf atoms introduces holes in the valence band formed of oxygen 2p levels. This leads to the splitting of the valence band and formation of high-spin defect states, causing the FM order for short V_{Hf}–V_{Hf} distances. On the other hand, the first-principles calculations of Zheng at al. [10], performed on undoped monoclinic HfO_2, showed that there are no stable defects that can carry a magnetic moment and confirmed that it is unlikely that hafnia vacancies are formed since their formation energy is high. From the above cited reports, it can be summarized that the appearance of ferromagnetism in hafnium oxide and its origin, still remains a matter of debate and deserves further investigation.

In the present work, we report room temperature ferromagnetism in Y-doped HfO_2 nanopowders. The ferromagnetic ordering is dependent on the crystal structure changes induced by Y. To the best of our knowledge, magnetic properties of hafnia nanopowders doped with yttrium have not been studied yet. HfO_2-based oxides, as high-*k* metal-oxide dielectrics, are already under consideration to replace silicon dioxide as gate dielectric for next generation of complementary metal-oxide semiconductors. The combination of ferromagnetic response at room temperature and above with dielectric properties of HfO_2-based oxides should enable the integration of metal-oxide semiconductors with spintronics technology. Therefore, Y-doped HfO_2 can be a promising candidate for the applications in spintronics.

2. Experiment

A highly pure, nanosized yttrium doped HfO_2 powders ($Hf_{1-x}Y_xO_{2-\delta}$, $0.05 \le x \le 0.2$) are obtained by metathesis synthesis described in detail elsewhere [11]. Starting chemicals were hafnium chloride ($HfCl_4$), yttrium nitrate hexahydrate ($Y(NO_3)_3 \cdot 6H_2O$) and sodium hydroxide (NaOH) from Alfa Aesar GmbH, Germany. The purity of starting chemicals was 99.9% without any magnetic ion impurity presence (such as Fe, Co etc.). The samples were always handled with Teflon tweezers to avoid any metal contamination. The compositions of the starting reacting mixtures were calculated according to the nominal composition of the final reaction product. Yttrium doped hafnia solid solutions were prepared varying weight fraction of yttrium (Y) in the range 5–20 mol%. All samples were annealed at 600 °C for 5 min in order to obtain better crystallinity. The obtained $Hf_{1-x}Y_xO_{2-\delta}$ nanopowders were characterized using different methods.

The X-ray diffraction (XRD) spectra of the samples have been measured on a Simens X-ray Diffractometer (Kristaloflex 500) with Ni filtered CuKα radiation. The room temperature measurements were performed in the 2θ range from 20° to 80° in a continuous scan mode with a step width of 0.02° and at a 2θ scanning rate of 1°/min.

Non-contact atomic force microscopy (NC-AFM) measurements were carried out using Omicron B002645 SPM probe VT AFM 25. NC-AFM images were obtained in the constant frequency shift mode (−20 Hz) and with constant vibrating amplitude (0.2 V).

Micro-Raman scattering measurements were performed at room temperature using a Jobin-Yvon T64000 triple spectrometer system and Ar^+/Kr^+ mixed laser line of 488 nm as an excitation source. The incident laser power was kept low (less than 10 mW) in order to prevent heating effects.

X-ray photoelectron spectroscopy (XPS) was used for the oxidation state and atomic ratio analysis. XPS was carried out on a PHI Quantera equipment with a base pressure in the analysis chamber of 10^{-9} Torr. The X-ray source was monochromatized AlKα radiation (1486.6 eV). The spectra were calibrated using the C 1s line (284.8 eV) of the adsorbed hydrocarbon on the sample surface.

The magnetic properties of the $Hf_{1-x}Y_xO_{2-\delta}$ samples were performed on a vibrating sample magnetometer in a high field measuring system (HFMS, Cryogenic Ltd).

3. Results and discussion

X-ray diffraction spectra of pure and Y-doped HfO_2 samples are presented in Fig. 1a. The XRD spectra of pure HfO_2 and $Hf_{1-x}Y_xO_{2-\delta}$ samples up to 10% of Y, show the monoclinic and tetragonal phase coexistence. With further increasing Y content, in 15% and 20% Y-doped samples the cubic phase appears. The main reflections of the monoclinic, tetragonal and cubic phases are marked with M, T and C in Fig. 1a. All diffraction peaks for the M, T and C phases in pure and Y-doped HfO_2 samples are indexed with the $P2_1/c$, $P4_2/nmc$ and Fm3m space group, respectively. The lattice parameters of the monoclinic, tetragonal and cubic phases are given in Table 1.

The volume fractions of different hafnia polymorphs in undoped and Y-doped HfO_2 samples were estimated from the integrated intensities of the M (−111), M (111) and T (111) diffraction peaks following the procedure proposed by Toraya et al. [12]. The estimated volume fractions for HfO_2 and Y-doped samples (given in %) are presented in Table 1.

As can be seen from Fig. 1a and Table 1, the monoclinic phase prevails over the tetragonal phase in pure HfO_2 sample. The XRD peaks are broadened which is characteristic of small (about 5 nm), oxygen deficient nanocrystals [11]. The XRD patterns of the Y-doped HfO_2 samples (labeled as HfY5-HfY20 according to the mol% of yttrium in doped samples) indicate the formation of solid solutions in the entire dopant compositional range without a presence of yttrium oxide or hydroxide phases. The yttrium substitution of Hf (Y_{Hf}) introduces oxygen vacancies in hafnia lattice and induces crystal structure changes of the HfO_2 nanopowders. The

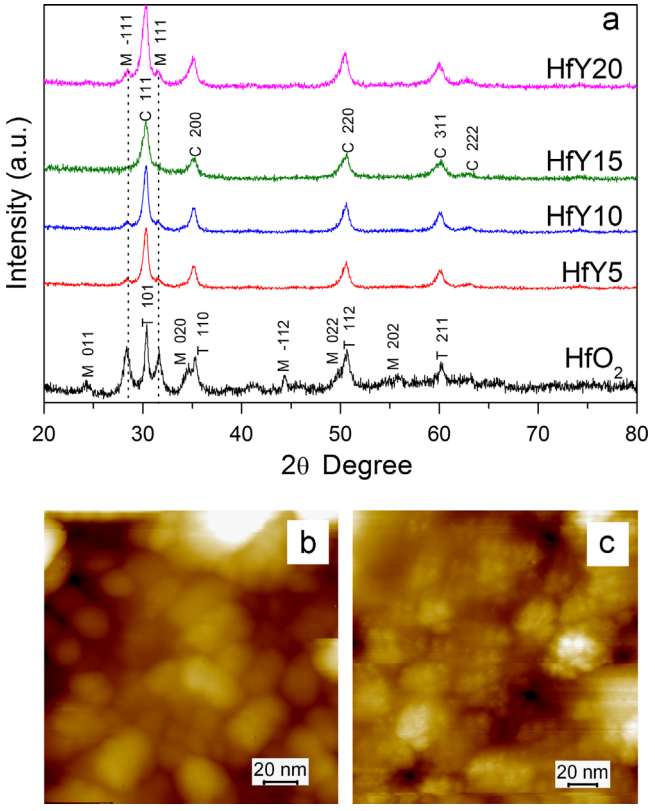

Fig. 1. (a) XRD patterns of Y-doped HfO_2 nanopowders at room temperature. The pure HfO_2 sample is given as a reference. The symbols stand for: M-monoclinic, T-tetragonal and C-cubic phase. The corresponding AFM images of (b) HfY10 and (c) HfY15 samples are presented.

Table 1
Composition and cell parameters of HfY samples obtained from XRD measurements.

Sample	Monoclinic $P2_1/c$				Tetragonal $P4_2/nmc$			Cubic $Fm3m$	
	(%)	a	b	c	(%)	a	c	(%)	a
HfY0	58	5.1453	5.1788	5.2919	42	3.5994	5.1191	–	–
HfY5	21	5.1418	5.1613	5.2928	79	3.6103	5.0980	–	–
HfY10	14	5.1265	5.1416	5.2830	86	3.6009	5.1835	–	–
HfY15	3	5.1169	5.1686	5.2967	46	3.6086	5.1800	51	5.1003
HfY20	16	5.1250	5.1797	5.2945	58	3.5737	5.1462	26	5.1166

structural transformation from monoclinic to tetragonal and cubic phase is a consequence of combined effect of doping with a lower valence state dopant and oxygen deficiency [2,3,11]. In the HfY5 sample the intensity of monoclinic reflections decreases implying that the content of monoclinic phase decreases on account of the tetragonal phase. This trend is even more pronounced for the HfY10 sample. In a case of the HfY15 sample, the XRD peaks which belong to M-phase are not visible anymore. The position of main diffraction peaks at 30.35°, 35.20°, 50.63° and 60.17° indicate that the cubic phase is formed [13] as dominant phase in this sample (see Table 1).

The tetragonal-cubic phase transformation is difficult to follow by an XRD method because of very low sensitivity of this method to the structural changes induced by oxygen displacement and nonstoichiometry. However, disappearance of M-phase, position of diffraction peaks and their significant broadening in a case of the HfY15 sample indicate the tetragonal-cubic phase transformation, as suggested by Fujimori and coauthors [14]. For the HfY20 sample, the content of T and M phases increases on the account of the cubic phase. This fact was somehow surprising because the cubic phase in HfO_2 is stabilized around 18 mol% of yttrium [15] or even less [16].

The morphology of the Y-doped nanopowders was analyzed by an AFM method. The AFM images of HfY10 and HfY15 samples, given in Fig. 1b and c, showed that the $Hf_{1-x}Y_xO_{2-\delta}$ nanopowders are composed of very small and agglomerated particles.

Raman scattering is much more sensitive method than the XRD to the structural changes induced by oxygen displacement and is powerful tool to investigate the tetragonal-cubic phase transformation in Y-doped HfO_2. The Raman spectra of $Hf_{1-x}Y_xO_{2-\delta}$ samples are shown in Fig. 2.

All Raman modes in HfY5 sample can be assigned to the monoclinic phase [17] except the mode at 500 cm^{-1} (marked as M/T1 in Fig. 2), which is also characteristic for the tetragonal phase [14]. The Raman modes are broadened because of the increased oxygen vacancy concentration when hafnia is doped with trivalent ions like Y [15]. With further increase of the Y content in the HfY10 sample, the Raman modes become broader implying that oxygen vacancy concentration further increases. New modes (marked as T2 and T3 in Fig. 2) appear and can be ascribed to the tetragonal phase [18]. The Raman mode denoted with asterisk (*) at ~190 cm^{-1} can originate from a small amount of γ-phase of HfO_2. The γ-phase can be identified only by Raman scattering [15]. In the HfY15 sample, the intensity of the Raman peaks which belong to the monoclinic and tetragonal phase decreases and the Raman modes became smeared out. Intensity drop of the mode at ~500 cm^{-1} reflects the tetragonal-cubic phase transition [14]. The F_{2g} mode of C-phase is not seen, because it is usually of very low intensity [17]. In the Raman spectrum of the HfY20 sample, the modes of T-phase became

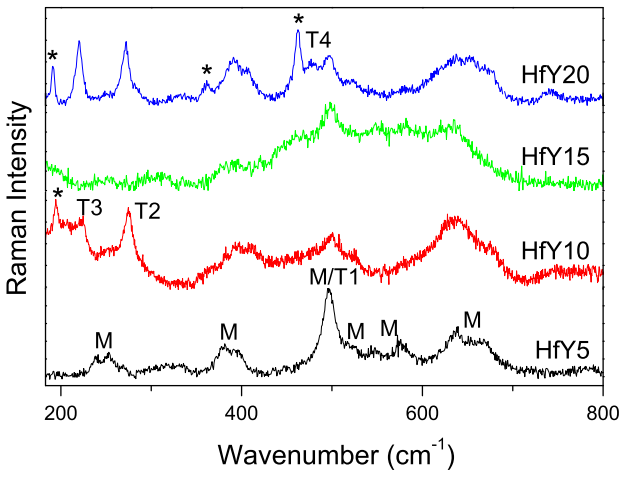

Fig. 2. Raman spectra of $Hf_{1-x}Y_xO_{2-\delta}$ ($0.05 \le x \le 0.2$) samples. The bands of monoclinic and tetragonal phases are designated by M, T1, T2, T3 and T4. Additional modes which can originate from γ-HfO_2 and cubic Y_2O_3 phases are denoted by asterisk (*).

more intensive than the modes of M-phase implying that the T-phase is dominant phase in this sample. This is in accordance with the XRD results. Additional modes at 360 cm^{-1} and 460 cm^{-1} can be ascribed to the cubic-Y_2O_3 phase probably formed at the nanoparticle surface [19].

The chemical state and composition of the $Hf_{1-x}Y_xO_{2-\delta}$ nanopowders were studied by XPS analyses. The XPS spectra of Hf 4f, O 1s and Y 3d region for Y-doped samples are given in Fig. 3a–c.

The deconvolution of the Hf 4f, O 1s and Y 3d spectra is performed for Y-doped samples using mixed Gaussian and Lorentzian functions. In Fig. 4a–c are presented deconvoluted XPS spectra of Hf 4f, Y 3d and O 1s region in a case of HfY5 sample for brevity.

The same procedure is applied for the rest of the samples and the binding energies (BE) of the most prominent XPS transitions

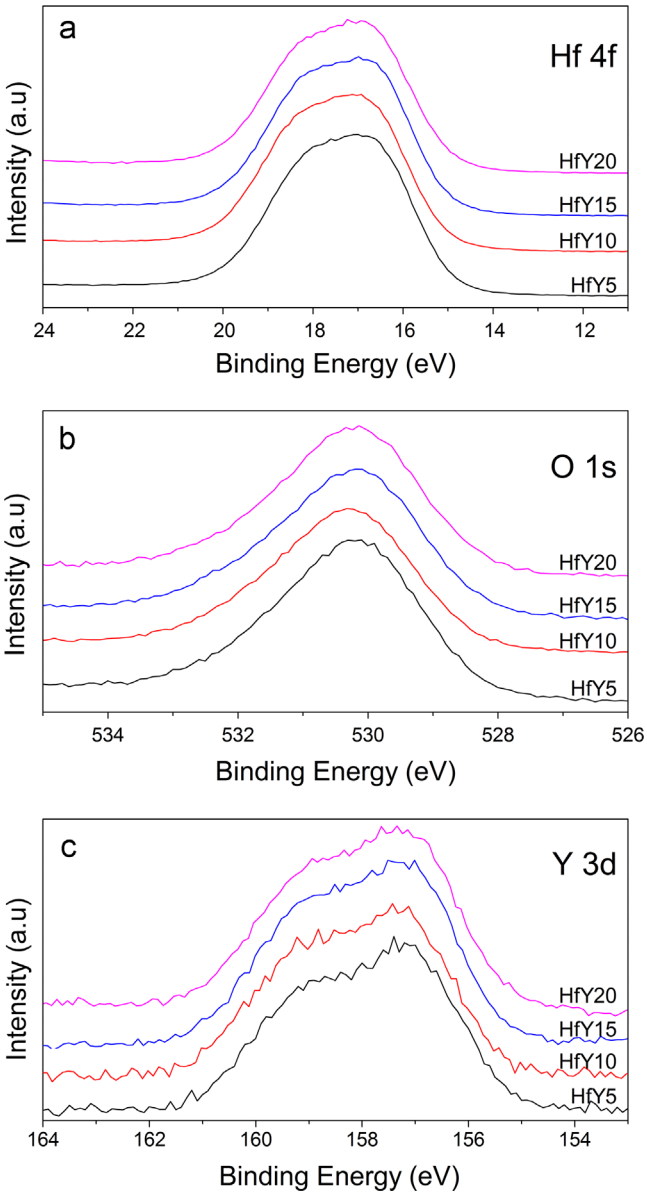

Fig. 3. The XPS spectra of (a) Hf 4f, (b) O 1s and (c) Y 3d region for Y-doped HfO_2 nanopowders.

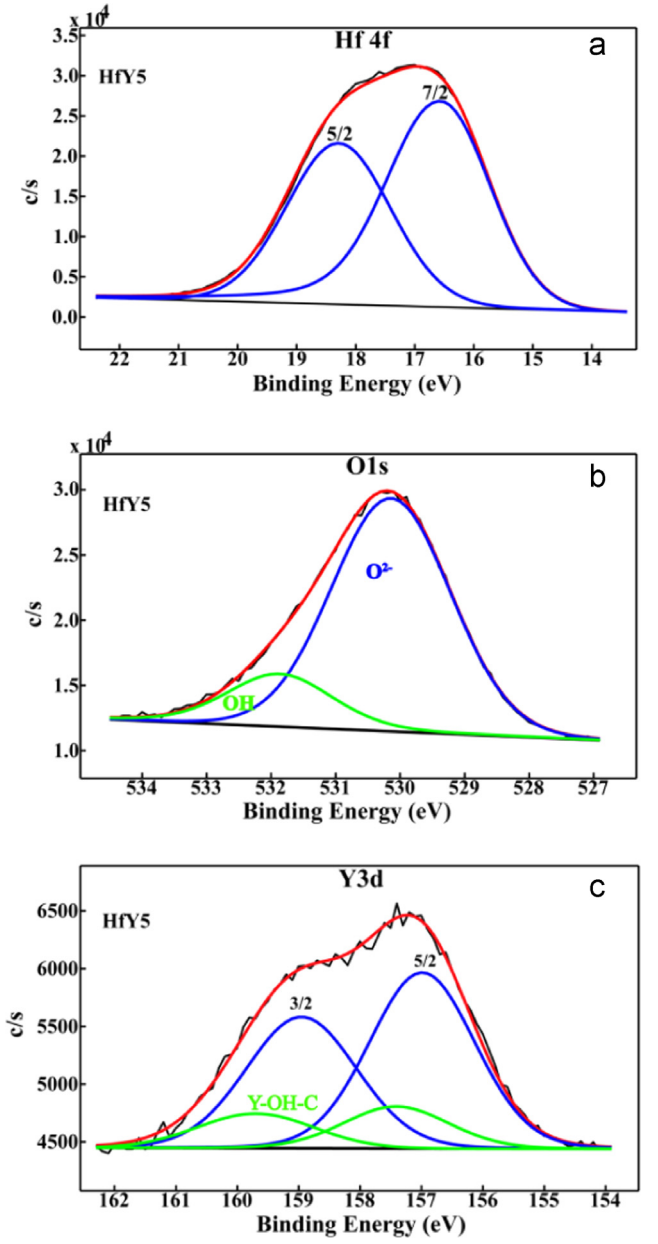

Fig. 4. Deconvoluted XPS spectra of (a) Hf 4f, (b) O 1s and (c) Y 3d region for HfY5 sample.

(Hf 4f, Y 3d, O 1s and C 1s) for $Hf_{1-x}Y_xO_{2-\delta}$ nanopowders are summarized in Table 2. No other contamination except carbon was detected in all investigated samples. XPS analysis of H 4f and O 1s gave evidence that the $Hf_{1-x}Y_xO_{2-\delta}$ samples are nonstoichiometric. From the O/Hf ratio, given in Table 2, it can be seen that the oxygen-deficiency increases with increasing Y content, with the exception of the HfY20 sample. This fact can be explained by the formation of the cubic-Y_2O_3 phase, already seen in the Raman spectrum of this sample.

The cations relative concentration for $Hf_{1-x}Y_xO_{2-\delta}$ samples, presented in Table 3, confirmed very good agreement between the surface and the nominal (bulk) stoichiometry. The errors regarding the quantitative data are found in the range of $\pm 10\%$, whereas the accuracy for BEs assignments is ± 0.2 eV.

Table 2
XPS binding energies (eV) of the individual peaks and composition of the HfY samples.

Sample	C 1s	O 1s		Hf 4f		Y 3d		Y–OH–C		Stoichiometry
		O^{2-}	OH	7/2	5/2	5/2	3/2			O/Hf
HfY5	284.8	530.1	531.8	16.6	18.3	156.9	159.0	157.4	159.6	1.9
HfY10	284.8	530.2	531.9	16.7	18.4	157.0	159.1	157.5	159.8	1.8
HfY15	284.8	530.1	531.9	16.6	18.3	157.0	158.9	157.5	159.8	1.83
HfY20	284.8	530.1	531.8	16.7	18.4	157.0	159.1	157.4	159.7	1.95

Table 3
Composition of HfY samples.

Sample	Y3d at%	Hf4f at%
HfY5	4.9	95.1
HfY10	9.3	90.7
HfY15	14.6	85.4
HfY20	19.1	80.9

The Hf 4f spectrum from Fig. 4a is composed of two spin-orbit doublet peaks (Hf $4f_{5/2}$ and Hf $4f_{7/2}$) which originate from the Hf bound to the oxygen. The Hf $4f_{7/2}$ peak is situated at 16.6 eV with a difference of 1.7 eV in binding energy between doublets. This peak is shifted to higher binding energies compared to the HfO_2 standard powdered sample (16.2 eV) [20] in all Y-doped samples (see Table 2). The higher binding energies of Hf $4f_{7/2}$ peak in Y-doped samples suggest that these nanopowders are deficient in oxygen and are non-stoichiometric [21,22]. The primary peak at 530.1 eV in the O 1s spectrum of Y-doped samples (see Fig. 4b and Table 2) is also shifted towards higher BE. This peak is ascribed to the oxygen bonded into the lattice and exhibits the shift probably because of the oxygen deficiency in the samples. Another subpeak in the O 1s spectrum at 531.8 eV (see Table 2) is assigned to adsorbed OH groups in the outermost surface layer [23,24]. The deconvoluted XPS spectrum of the Y 3d doublet ($3d_{5/2}$ and $3d_{3/2}$) is presented in Fig. 4c for the HfY5 sample. The average positions of the Y $3d_{5/2}$ peaks in $Hf_{1-x}Y_xO_{2-\delta}$ samples are given in Table 2 and are located around 157 eV. These peaks are slightly shifted to higher energy compared to the position of $3d_{5/2}$ peak in Y_2O_3 standard sample (156.5 eV) [20]. The shift to higher BE is expected if we have the formation of the Hf–Y–O bonds [16]. The fitting of the Y 3d spectra of doped samples requires additional doublet (binding energies are given in Table 2). The second doublet can be attributed to Y–OH–C bonds confined to the surface as a result of the OH and hydrocarbon adsorption from the atmosphere.

In summary, XPS and Raman analysis of the $Hf_{1-x}Y_xO_{2-\delta}$ samples confirmed that yttrium doping increases the concentration of oxygen vacancies, whereas XRD and Raman results showed that the incorporation of yttrium induces structural phase transformation. These findings are in agreement with Manory et al. [13] who reported that tetragonal and cubic phase of HfO_2 are stable at room temperature in nonstoichiometric HfO_2. In Fig. 5 we gave an illustration of the phase transformation in HfO_2 with Y doping. In Fig. 5a is presented the monoclinic phase of nonstoichiometric undoped HfO_2 with three- and four-coordinated oxygen vacancies. Yttrium as a dopant ion in 3^+ valence state brings additional vacancies in the hafnia lattice in order to keep the charge neutrality (Fig. 5b). With further addition of Y, the concentration of the oxygen vacancies should be increased and the monoclinic phase of HfO_2 transforms first into the tetragonal and then into the cubic phase as presented in Fig. 5c and d.

The room temperature magnetization versus magnetic field (M–H) data for pure HfO_2 and Y-doped samples is shown in Fig. 6a. It can be seen that all samples show a ferromagnetic signal at room temperature superimposed onto a diamagnetic background. The observed ferromagnetism is characteristic for the nanostructured nature of the investigated samples [25] and is intrinsic as there are no magnetic impurities present in the samples (see experimental part). The susceptibility of the diamagnetic component, i.e. the slope of the high-field parts of the curve, remains constant with yttrium doping because of the closed Y^{3+} shells. After subtracting the diamagnetic component, the corrected magnetization curves are shown in Fig. 6b. The magnetization curves are almost anhysteretic, as it is often the case for ferromagnetic oxides [26]. The saturation magnetization value (M_S) for the undoped sample is about 2.2×10^{-3} emu g^{-1}. The obtained value is comparable with the other reports on ferromagnetism in undoped oxide nanocrystals [25–29], but higher than the reported value on HfO_2 powders [5]. The value of M_S increases for the HfY5 sample and reaches its maximum of 2.9×10^{-3} emu g^{-1} for the HfY10 sample. The saturation magnetization significantly drops off in the HfY15 and HfY20 samples to the values of 1.2×10^{-3} emu g^{-1} and 0.7×10^{-3} emu g^{-1} respectively. The change of the M_S for pure HfO_2 and $Hf_{1-x}Y_xO_{2-\delta}$ samples is presented in Fig. 6c.

The experimental reports [30–33] confirmed the existence of RTFM in pure and doped hafnia films and clearly proved that the RTFM originates from the presence of oxygen vacancies. The lack of oxygen vacancies or filling up vacancies can degrade or even completely destroy the FM ordering. Scarce literature data concerning the appearance of the FM in other hafnia nanostructures like nanopowders or nanorods [33–35] have also pointed out that the oxygen vacancies play a major role in the magnetic exchange mechanism. The appearance of RTFM in pure HfO_2 can be interpreted in the framework of the impurity band exchange model proposed by Venkatesan et al. [4]. According to this model, the intrinsic oxygen vacancies act as a donor of electrons, leading to the n-type doping of the hafnia. The electrons trapped in oxygen vacancies in HfO_2 form extended hydrogen-like orbitals because of the relatively high dielectric constant of hafnia. When the defect

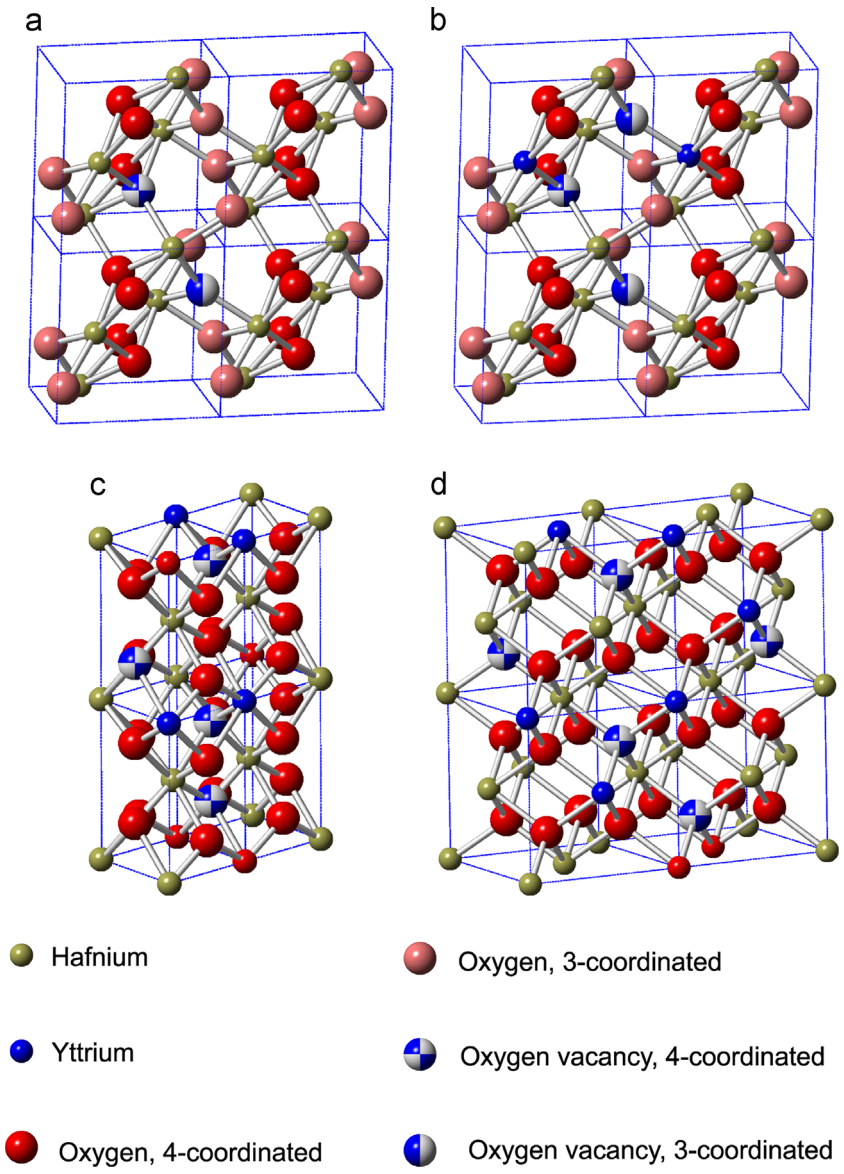

Fig. 5. Structural phase transformation with Y doping (a) pure HfO_2 monoclinic phase, (b) monoclinic phase of HfO_2 doped with Y, (c) tetragonal phase and (d) cubic phase of HfO_2 with increased Y content.

concentration increases, the overlapping of the defect-related orbitals can form an impurity (defect) band. The mixing of the defect band with empty 5d states of hafnia enables the transfer of some of the electrons to the 5d band. The 5d electrons will in turn polarize the defect band establishing the ferromagnetic coupling [4]. The oxygen vacancies in monoclinic hafnia can be in different charge states having different number of trapped electrons and bearing different magnetic moment [7,36]. Some of these defects like negatively (V_O^-) or positively (V_O^+) charged vacancies form levels near the conduction band, as shown in the paper of Xiong et al. [36]. They calculated the energy levels of the oxygen vacancy defects in different charge states for HfO_2 and showed that the energy levels of the V_O^- and V_O^+ defects lie very near to the conduction band (approximately at 0.8 and 1.1 eV below the conduction band edge). Consequently, it is reasonable to assume that the defect band, formed from V_O^- and V_O^+ states, will lie near the conduction band. The fraction of the electrons from defect band can be transferred to the 5d states causing the spin splitting of the defect band. The formation of the spin-split defect band provides necessary condition for the appearance of ferromagnetism [4]. In Fig. 7a is given the schematic representation of the defect levels induced by oxygen vacancies in different charge states according to the calculations performed in Ref. [34]. The mixing of the defect band with the 5d states of hafnia and its spin-splitting is presented in Fig. 7b.

Having in mind theoretical calculations [7,36] and experimental observations [30–33] and knowing from the Raman and XPS results that $Hf_{1-x}Y_xO_{2-\delta}$ nanopowders are oxygen deficient, we concluded that the oxygen vacancies can be attributed to be the main source of ferromagnetism in undoped and Y-doped HfO_2 nanopowders. In the HfY5 sample, with Y doping the concentration of oxygen vacancies should increase (see Fig. 5b) in order to

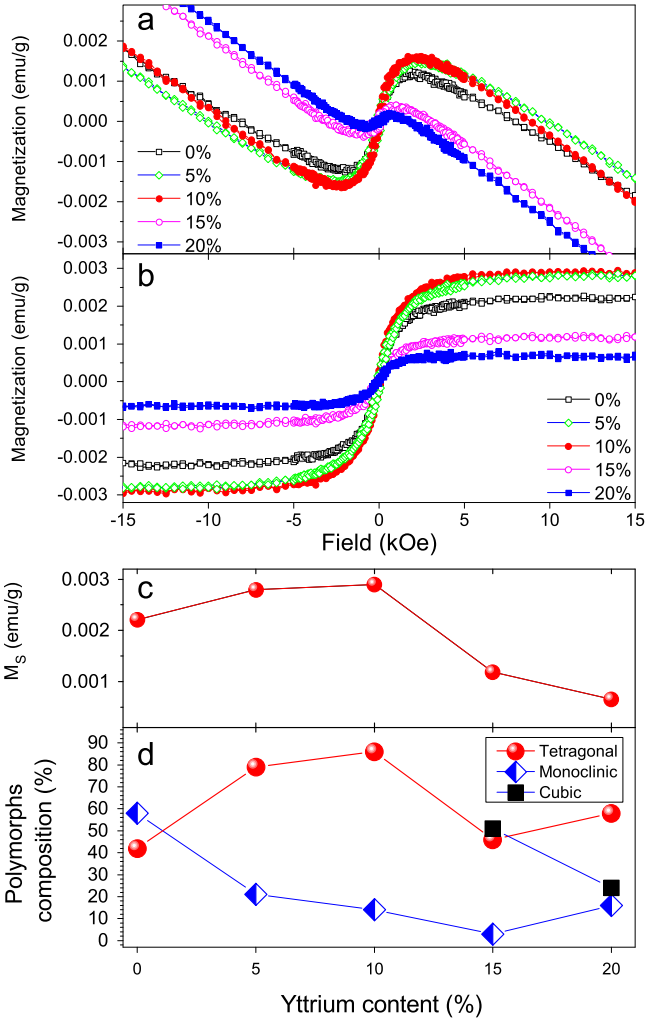

Fig. 6. Magnetic properties of $Hf_{1-x}Y_xO_{2-\delta}$ samples. (a) Raw magnetization curves versus magnetic field, $M(H)$, (b) $M(H)$ after subtraction of the linear diamagnetic component, (c) Saturation magnetization (M_S) change and (d) relative polymorph composition change with yttrium content.

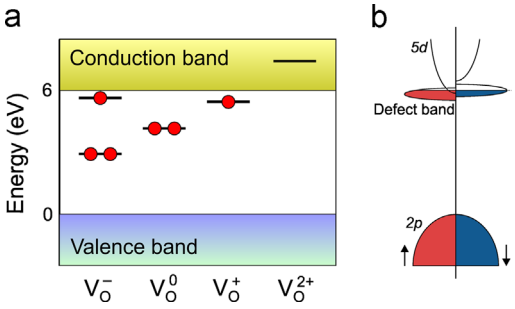

Fig. 7. Schematic representation of the (a) defect levels which originate from point defects and (b) a spin-split defect band.

keep electroneutrality. At the same time the content of tetragonal phase begins to prevail over the monoclinic one. The FM signal is stronger than that in undoped HfO_2. With increasing Y content up to 10%, the saturation magnetization and the strength of FM ordering further increase, when the content of the tetragonal phase in HfY10 sample becomes dominant (Fig. 5c). In the HfY15 sample the cubic phase appears and the strength of FM interaction weakens, reaching the lowest value of M_S (0.7×10^{-3} emu g^{-1}) for HfY20. This value of M_S is almost three times lower than for HfY10 sample. From the change of the polymorphs composition with increasing Y content presented in Fig. 6d, it can be seen that the change of M_S and T-phase content have similar trend. In a case of HfY20 sample, M_S continues to decrease despite the fact that the amount of T-phase is slightly increased.

The theoretical calculations performed by Chen et al. [37] can offer the explanation for the degradation of FM ordering in HfY15 and HfY20 samples. Namely, Chen et al. [37] calculated the formation energies of the oxygen vacancies in different charge states for Y-doped cubic HfO_2. It is found that with higher Y content, oxygen vacancies form complex defects with yttrium (V_O–Y_{Hf}) in different charge states ((V_O–$Y_{Hf})^+$, (V_O–$Y_{Hf})^{++}$ and (V_O–$Y_{Hf})^0$ complexes). Among these complexes, the single positively charged complexes (V_O–$Y_{Hf})^+$ are the most stable ones. Y as dopant changes the charge state of oxygen vacancies and lowers the highest occupied levels induced by V_O^+ and V_O^{++} vacancies into the valence band. Therefore, the highest occupied levels of (V_O–$Y_{Hf})^+$ and (V_O–$Y_{Hf})^{++}$ complex defects will lie in the vicinity of the valence band. With further increasing of Y content the highest occupied levels of (V_O–$Y_{Hf})^0$ complexes would also fall into the valence band [37]. Considering the results from Ref. [37], it is reasonable to assume that in HfY15 and HfY20 samples, because of the increased Y content and the presence of cubic phase, certain number of (V_O–Y_{Hf}) defect complexes can be formed. The appearance of (V_O–Y_{Hf}) defect complexes will degrade the ferromagnetic interaction because the defect band formed from (V_O–Y_{Hf}) complex defects states will lie near to the valence band. The mechanism of electron transfer from defect band to 5d empty states which leads to its polarization and establishing of ferromagnetic interaction is not applicable anymore. The formation of cubic-Y_2O_3 phase at nanoparticle surface, seen in the Raman spectrum of HfY20 sample can explain further degradation of ferromagnetism in this sample.

4. Conclusions

In summary, nonstoichiometric $Hf_{1-x}Y_xO_{2-\delta}$ nanosized powders ($0 \le x \le 0.2$) are obtained by metathesis synthesis. The transformation of crystal structure from monoclinic to tetragonal and cubic phase (M→T→C) with increased Y doping was confirmed by XRD and Raman measurements. The XPS and Raman studies testified that the $Hf_{1-x}Y_xO_{2-\delta}$ nanopowders are nonstoichiometric. All samples exhibit room temperature ferromagnetism which increases with increased tetragonal phase content and degrades with the appearance of cubic phase. The FM ordering in $Hf_{1-x}Y_xO_{2-\delta}$ samples can be explained in the framework of impurity band exchange model where oxygen vacancies in different charge state, as n-type dopants, play major role in establishing ferromagnetism. Further increasing of Y content stabilizes the cubic phase in 15% and 20% Y doped samples and the ferromagnetic interaction weakens. In a cubic phase certain number of oxygen vacancy-yttrium complexes (V_O–Y_{Hf}) can be formed. Those complexes form defect states inside the

bandgap of hafnia. The highest occupied defect states will lie in the vicinity of the valence band. The electron transfer from deep lying defect states to the 5d empty states of hafnia, which enables the establishing of ferromagnetic interaction is not realistic anymore. The presence of cubic-Y_2O_3 phase additionally degrades ferromagnetic ordering in the 20% Y doped sample.

Acknowledgments

This work was financially supported by the Ministry of Education, Science and Technological Development of the Republic of Serbia under the projects ON171032 and III45018. Dr Rareş Scurtu acknowledges the support of the Sectorial Operational Programme Human Resource Development (SOPHRD) under the contract number POSDRU/89/1.5/S/63700.

References

[1] R. Ruh, V.A. Patel, Proposed phase relations in the HfO_2-rich portion of the system Hf-HfO_2, J. Am. Ceram. Soc. 56 (1973) 606–607.
[2] E. Rauwel, C. Dubourdieu, B. Hollander, N. Rochat, F. Ducroquet, M.D. Rossell, G. Van Tendeloo, B. Pelissier, Stabilization of the cubic phase of HfO_2 by Y addition in films grown by metal organic chemical vapor deposition, Appl. Phys. Lett. 89 (2006) 012902.
[3] L. Gao, L. Zhou, J. Feng, L. Bai, C. Li, Z. Liu, J.-L. Soubeyroux, Y. Lu, Stabilization of cubic structure in Mn-doped hafnia, Ceram. Int. 38 (2012) 2305–2311.
[4] M. Venkatesan, C.B. Fitzgerald, J.M.D. Coey, Thin films: unexpected magnetism in a dielectric oxide, Nature 430 (2004) 630.
[5] J.M.D. Coey, M. Venkatesan, P. Stamenov, C.B. Fitzgerald, L.S. Dorneles, Magnetism in hafnium dioxide, Phys. Rev. B 72 (2005) 024450.
[6] M.D. Glinchuk, E.A. Eliseev, V.V. Khist, A.N. Morozovska, Ferromagnetism induced by magnetic vacancies as a size effect in thin films of nonmagnetic oxides, Thin Solid Films 534 (2013) 685–692.
[7] D. Muñoz Ramo, J.L. Gavartin, A.L. Shluger, G. Bersuker, Spectroscopic properties of oxygen vacancies in monoclinic HfO_2 calculated with periodic and embedded cluster density functional theory, Phys. Rev. B 75 (2007) 205336.
[8] C. Das Pemmaraju, S. Sanvito, Ferromagnetism driven by intrinsic point defects in HfO_2, Phys. Rev. Lett. 94 (2005) 217205.
[9] J.I. Beltrán, M.C. Muñoz, J. Hafner, Structural, electronic and magnetic properties of the surfaces of tetragonal and cubic HfO_2, New J. Phys. 10 (2008) 063031.
[10] J.X. Zheng, G. Ceder, T. Maxisch, W.K. Chim, W.K. Choi, First-principles study of native point defects in hafnia and zirconia, Phys. Rev. B 75 (2007) 104112.
[11] B. Matović, D. Bučevac, M. Prekajski, V. Maksimović, D. Gautam, K. Yoshida, T. Yano, Synthesis and characterization of nanometric yttrium-doped hafnia solid solutions, J. Eur. Ceram. Soc. 32 (2012) 1971–1976.
[12] H. Toraya, M. Yoshimura, S. Somiya, Calibration curve for quantitative analysis of the monoclinic-tetragonal ZrO_2 system by X-ray diffraction, J. Am. Ceram. Soc. 67 (1984) C-119–C-121.
[13] R.R. Manory, T. Mori, I. Shimizu, S. Miyake, G. Kimmel, Growth and structure control of HfO_{2-x} films with cubic and tetragonal structures obtained by ion beam assisted deposition, J. Vac. Sci. Technol. A 20 (2002) 549–554.
[14] H. Fujimori, M. Yashima, S. Sasaki, M. Kakihana, T. Mori, M. Tanaka, M. Yoshimura, Cubic–tetragonal phase change of yttria-doped hafnia solid solution: high-resolution X-ray diffraction and Raman scattering, Chem. Phys. Lett. 346 (2001) 217–223.
[15] M. Yashima, H. Takahashi, K. Ohtake, T. Hirose, M. Kakihana, H. Arashi, Y. Ikuma, Y. Suzuki, M. Yoshimura, Formation of metastable forms by quenching of the HfO_2–$RO_{1.5}$ melts (R=Gd, Y and Yb), J. Phys. Chem. Solids 57 (1996) 289–295.
[16] C. Dubourdieu, E. Rauwel, H. Roussel, F. Ducroquet, B. Hollander, M. Rossell, G. Van Tendeloo, S. Lhostis, S. Rushworth, Addition of yttrium into HfO_2 films: microstructure and electrical properties, J. Vac. Sci. Technol. A 27 (2009) 503–514.
[17] X. Zhao, D. Vanderbilt, First-principles study of structural, vibrational, and lattice dielectric properties of hafnium oxide, Phys. Rev. B 65 (2002) 233106.
[18] G.M. Rignanese, X. Gonze, G. Jun, K. Cho, A. Pasquarello, First-principles investigation of high-κ dielectrics: comparison between the silicates and oxides of hafnium and zirconium, Phys. Rev. B 69 (2004) 184301.
[19] A. Ubaldini, M.M. Carnasciali, Raman characterisation of powder of cubic RE_2O_3 (RE=Nd, Gd, Dy, Tm, and Lu), Sc_2O_3 and Y_2O_3, J. Alloy. Compd. 454 (2008) 374–378.
[20] J.F. Moulder, W.F. Stickle, P.E. Sobol, K.D. Bomben, Handbook of X-ray Photoelectron Spectroscopy, Perkin-Elmer Corp, Minnesota, 1992.
[21] N. Selvakumar, H.C. Barshilia, K.S. Rajam, A. Biswas, Structure, optical properties and thermal stability of pulsed sputter deposited high temperature HfO_x/Mo/HfO_2 solar selective absorbers, Sol. Energy Mater. Sol. Cells 94 (2010) 1412–1420.
[22] G. He, M. Liu, L.Q. Zhu, M. Chang, Q. Fang, L.D. Zhang, Effect of postdeposition annealing on the thermal stability and structural characteristics of sputtered HfO_2 films on Si(1 0 0), Surf. Sci. 576 (2005) 67–75.
[23] X. Qiu, J.Y. Howe, H.M. Meyer Iii, E. Tuncer, M.P. Paranthaman, Thermal stability of HfO_2 nanotube arrays, Appl. Surf. Sci. 257 (2011) 4075–4081.
[24] J.C. Hackley, T. Gougousi, Properties of atomic layer deposited HfO_2 thin films, Thin Solid Films 517 (2009) 6576–6583.
[25] A. Sundaresan, C.N.R. Rao, Ferromagnetism as a universal feature of inorganic nanoparticles, Nano Today 4 (2009) 96–106.
[26] J.M.D. Coey, Dilute magnetic oxides, Curr. Opin. Solid State. Mater. Sci. 10 (2006) 83–92.
[27] M.Y. Ge, H. Wang, E.Z. Liu, J.F. Liu, J.Z. Jiang, Y.K. Li, Z.A. Xu, H.Y. Li, On the origin of ferromagnetism in CeO_2 nanocubes, Appl. Phys. Lett. 93 (2008) 062505.
[28] Z.D. Dohčević-Mitrović, N. Paunović, M. Radović, Z.V. Popović, B. Matović, B. Cekić, V. Ivanovski, Valence state dependent room-temperature ferromagnetism in Fe-doped ceria nanocrystals, Appl. Phys. Lett. 96 (2010) 203104.
[29] N. Paunović, Z. Dohčević-Mitrović, R. Scurtu, S. Aškrabić, M. Prekajski, B. Matović, Z.V. Popović, Suppression of inherent ferromagnetism in Pr-doped CeO_2 nanocrystals, Nanoscale 4 (2012) 5469–5476.
[30] Y.H. Chang, Y.L. Soo, W.C. Lee, M.L. Huang, Y.J. Lee, S.C. Weng, W.H. Sun, M. Hong, J. Kwo, S.F. Lee, J.M. Ablett, C.C. Kao, Observation of room temperature ferromagnetic behavior in cluster-free, Co doped HfO_2 films, Appl. Phys. Lett. 91 (2007) 082504.
[31] K.K. Bharathi, S. Venkatesh, G. Prathiba, N.H. Kumar, C.V. Ramana, Room temperature ferromagnetism in HfO_2 films, J. Appl. Phys. 109 (2011) 07C318.
[32] N.H. Hong, J. Sakai, N. Poirot, V. Brizé, Room-temperature ferromagnetism observed in undoped semiconducting and insulating oxide thin films, Phys. Rev. B 73 (2006) 132404.
[33] X. Liu, Y. Chen, L. Wang, D.-L. Peng, Transition from paramagnetism to ferromagnetism in HfO_2 nanorods, J. Appl. Phys. 113 (2013) 076102.
[34] M.K. Sharma, D.K. Mishra, S. Ghosh, D. Kanjilal, P. Srivastava, R. Chatterjee, Oxygen vacancy mediated large magnetization in chemically synthesized Ni-doped HfO_2 nanoparticle powder samples, J. Appl. Phys. 110 (2011) 063902.
[35] E. Tirosh, G. Markovich, Control of defects and magnetic properties in colloidal HfO_2 nanorods, Adv. Mater. 19 (2007) 2608–2612.
[36] K. Xiong, J. Robertson, M.C. Gibson, S.J. Clark, Defect energy levels in HfO_2 high-dielectric-constant gate oxide, Appl. Phys. Lett. 87 (2005) 183505.
[37] G.H. Chen, Z.F. Hou, X.G. Gong, Q. Li, Effects of Y doping on the structural stability and defect properties of cubic HfO_2, J. Appl. Phys. 104 (2008) 074101.